Surface Characterization of Lanthanum Aluminate ($LaAlO_3$)

Elizabeth Ann Steele

Advisers:
Professor Laurence Marks
Pratik Koirala
Dr. Kathleen Stair

Department of Materials Science and Engineering
Northwestern University
Evanston, Illinois

June 2016

Submitted in partial fulfillment of the requirements of the degree
Bachelor of Science with Honors

ACKNOWLEDGEMENTS

I have learned a great deal throughout the process of my undergraduate research, and it would not have been possible without support from many wonderful, intelligent, and patient people. First and foremost I thank Professor Laurence Marks who allowed me to join his research group as an undergraduate student. Professor Marks taught me that a TEM image is worth more than one thousand words (if it's good) and pushed me to gain experience on more equipment than I even knew existed.

I send endless thanks to Pratik Koirala for helping me out at every step of the way of my work. He trained me on everything from sample preparation to centered-dark field imaging to XPS analysis and provided assistance whenever I got stuck. He always holds me accountable for my fitness goals, and is a great friend. Dr. Ahmet Gulec performed microscopy on my samples at UIC and helped me do HRTEM in NUANCE. I thank him for his significant contribution of time and dedication. Say Cook performed steps of the sample preparation process at Argonne National Laboratory while equipment at NUANCE remained inaccessible for over four months. I thank him for his willingness to help during a time of frustration. I thank the rest of the Marks group for their mentorship in aspects of science and life over the past year and a half. I appreciate you welcoming me into your family. I am going to miss spending time with you and I doubt there is a friendlier group of graduate students around.

A tremendous amount of thanks is due to Dr. Kathleen Stair, "mother" of the undergraduate materials science students. Your leadership and advice were invaluable to me as I progressed through my Northwestern experience. I cannot thank you enough for everything you do for your students. I also thank the MSE undergraduate community at Northwestern for being the reason I got through classes with a smile and the reason I feel ready to face professional technical settings. We have gone from thinking we knew it all to realizing we might never really understand anything. Thank you for all the support, shared meals, and laughs.

Finally, I send thanks to my family members, who are the reason I am here today. You fostered in me a lifelong love of learning for which I am extremely grateful.

ABSTRACT

Perovskite materials such as lanthanum aluminate ($LaAlO_3$, LAO) can be used in heterogeneous catalysis as support oxides and active catalysts. Surface orientation and structure have been shown to influence catalytic activity and ordered growth. Because of the presence of high-energy "dangling bonds," a material's surface may form atomic or electronic "reconstructions." The bulk properties of $LaAlO_3$ are well understood and some surface reconstructions have been reported, while some orientations remain unexamined. This work presents initial characterizations of a model system, the LAO (111) surface, using methods including transmission electron microscopy (TEM) and x-ray photoelectron spectroscopy (XPS). The (111) samples are shown to preferentially facet, forming a (110) face. Observations of the edge are consistent with (nx1) reconstructions of the LAO (110) surface. Additionally, evidence of ordered surface structures on LAO (111) is presented. This work can be used as a basis for solving the exact structure of LAO (111) reconstructions.

Table of Contents

List of Figures

1. INTRODUCTION

Oxide materials have a wide range of applications and are commonly used in catalysis, electronic parts, and even building materials. The surfaces of oxides demand specific attention because of their functional importance, which cannot be understated. Active sites are found on the surface of catalysts and the structure of oxide support substrates determines catalyst properties. The surfaces of small electronic parts and devices become increasingly important as their surface-area-to-volume ratio decreases. The surface of a material is often the first line of defense against unfriendly environmental conditions. Despite the importance of surfaces, they are understood far less than the bulk structure of materials. The complexity of surfaces makes them a difficult but valuable area of study.

Oxide materials with similar bulk structures can be grouped together and studied. As shown in Figure 1, "Perovskite materials" or "perovskites" are oxides with the perovskite structure (ABO_3) in which A- and B-site cations are covalently bonded to oxygen. This work studies the structural behavior on the surface and edge of one perovskite structure, lanthanum aluminate ($LaAlO_3$, LAO), through use of electron microscopy and spectroscopy characterization methods. This introduction will describe applications of perovskites and justify studying the surface of $LaAlO_3$. Central concepts in surface science will be explained and the body of perovskite surface research will be briefly reviewed in order to frame the discussion of experimental work in subsequent chapters.

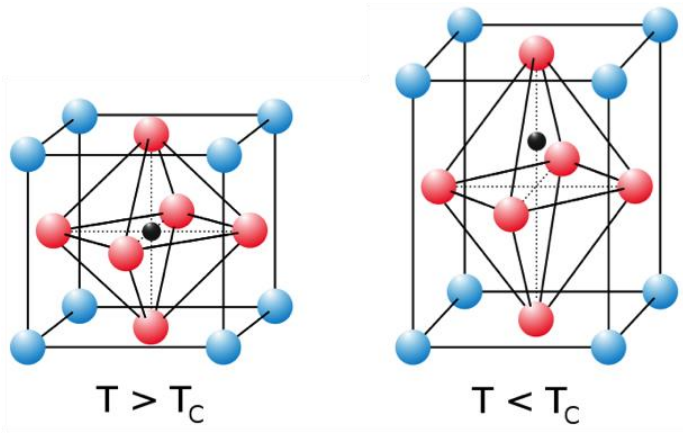

Figure 1. The ABO_3 perovskite structure is shown. For $LaAlO_3$, La^{3+} is the A-site cation (blue) and Al^{3+} is the B-site cation (black), both of which are covalently bonded to oxygen. Ideal perovskites have cubic structures (left image). In reality, structures are pseudocubic or form phases with orthorhombic, tetragonal, or rhombohedral structures. $LaAlO_3$ experiences a transition from a rhombohedral to a pseudocubic structure at T_c=500°C [1].

1.1 Perovskites in catalysis

The trillion-dollar global chemical industry fuels industries ranging from consumer goods to transportation to pharmaceuticals. According to the International Energy Agency (IEA), around 90% of all chemical reactions involve catalysts [2]. Heterogeneous catalysis, a process in which the phase of the catalyst differs from the phase of the reactants, is the dominant type of catalysis. The industrial prevalence of catalysts motivates research aimed at designing efficient, clean materials for catalysis.

Perovskite oxides are studied both as active and model catalysts. Hydrocarbon combustion, oxidative coupling of methane (OCM), and nitrogen oxide decomposition or reduction are all examples of chemical processes that use perovskite catalysts [3]. Perovskites are ideal for catalysis because of their stability at high temperatures and the availability of the A- and B-site cations for substitution in reactions. Precise study of catalytic reactions is difficult because of the high-pressure experimental conditions and use of catalysts in powder form. Active catalysts can be simulated by model catalytic systems such as flat single crystals with known crystallographic orientation. The use of model systems allows for simplified structural studies that still provide useful information about perovskite structure and properties. $LaAlO_3$ has been studied as a model catalyst and an active catalyst for more than 20 years [4-7]. It was first discovered to successfully catalyze oxidative coupling of methane (OCM) in 1986 by Imai and Tagawa [7]. $LaAlO_3$ and similar materials have been studied as industrial catalysts, sometimes after being doped with elements such as copper [8]. Overall, despite stability at a range of temperatures and types of reactions, perovskites have not yet been commercialized because of their low efficiency and sensitivity to toxic compounds such as SO_2 [9].

Oxides can also play a supporting role in catalysis. During heterogeneous catalysis, an oxide substrate referred to as a “support oxide” is the material to which a catalyst is affixed. The properties of the support oxide are significant because of the potential for interaction with both the catalyst and the reaction itself. In one recently studied system, in which strontium titanate ($SrTiO_3$, STO) nanocuboids supported Pd nanoparticles, it was shown that the growth of the Pd nanoparticles was dependent on the surface termination of STO [10]. The results of directional studies of perovskite surface model systems are applicable to systems in which the perovskite is the catalyst or the support oxide.

1.2 Thin-film growth and electronic heterostructures

Another area of interest for perovskite oxides is thin-film growth, specifically epitaxial growth, which involves the ordered deposition of a material on a substrate with matching crystallographic orientation. The structure and properties of the film depend greatly on the structure of the substrate. Perovskites can be the substrate or the deposited thin film. Perovskite thin films have a variety of applications including, as shown recently, use in solar cells [11]. $LaAlO_3$ has long been established as a substrate used for growth of other materials such as high temperature superconductors. LAO is an appealing material for further study in electronics applications because of its electrical and physical characteristics, namely its high dielectric constant (around 25), ability to be grown and studied as a thin film itself [12, 13], and compatibility with other electronic materials. Research has shown the promise of $LaAlO_3$ as a candidate for high-κ applications such as gate dielectrics [14].

LAO has gained attention in settings where it interacts with other materials. In 2004, Ohtomo and Hwang observed the presence of a high-mobility 2D electron gas at the LAO/STO heterostructure interface [15]. After this discovery, additional research revealed other interesting interface properties such as superconductivity [16, 17] and magnetic effects [18]. Ohtomo and Hwang's work provided motivation for studying the surface structure of $SrTiO_3$ and $LaAlO_3$ with hopes of connecting the observed properties with one or both of the material structures at the interface. In addition to interaction with STO, LAO has been studied theoretically and experimentally in other heterostructures such as $LaNiO_3/LaAlO_3$ superlattices. Studies of the electronic properties of (111) LNO/LAO super-lattices are the only time LAO (111) appears in literature [19-21]. A fuller understanding of the surface structure of LAO (111) is needed to fully understand the effect of the LAO surface on charge transport across the heterostructure and the further implications of these studies.

1.3 Other applications

In addition to catalysis and electronic applications, $LaAlO_3$ has been studied and tested for use in methane-fueled solid oxide fuel anodes [22] and as a thermal camouflaging material because of its ability to reduce infrared emissivity of fabric surfaces when applied as a thin film [23].

1.4 Crystallographic directions

In most materials, structure and properties depend on directionality. This concept can be simply demonstrated by examining a piece of clothing or fabric and observing the difference in elasticity when the material is pulled parallel and perpendicular to the fibers. In a crystalline material, directionality is significant because atomic stacking changes with orientation. Figure 2 shows views of the cross section and different atomic layers for three orientations of $LaAlO_3$. It is necessary to keep orientation in mind as a parameter when selecting materials systems for practical use and research. The use of single crystal samples (see section 2.1) allows the study of one orientation at a time.

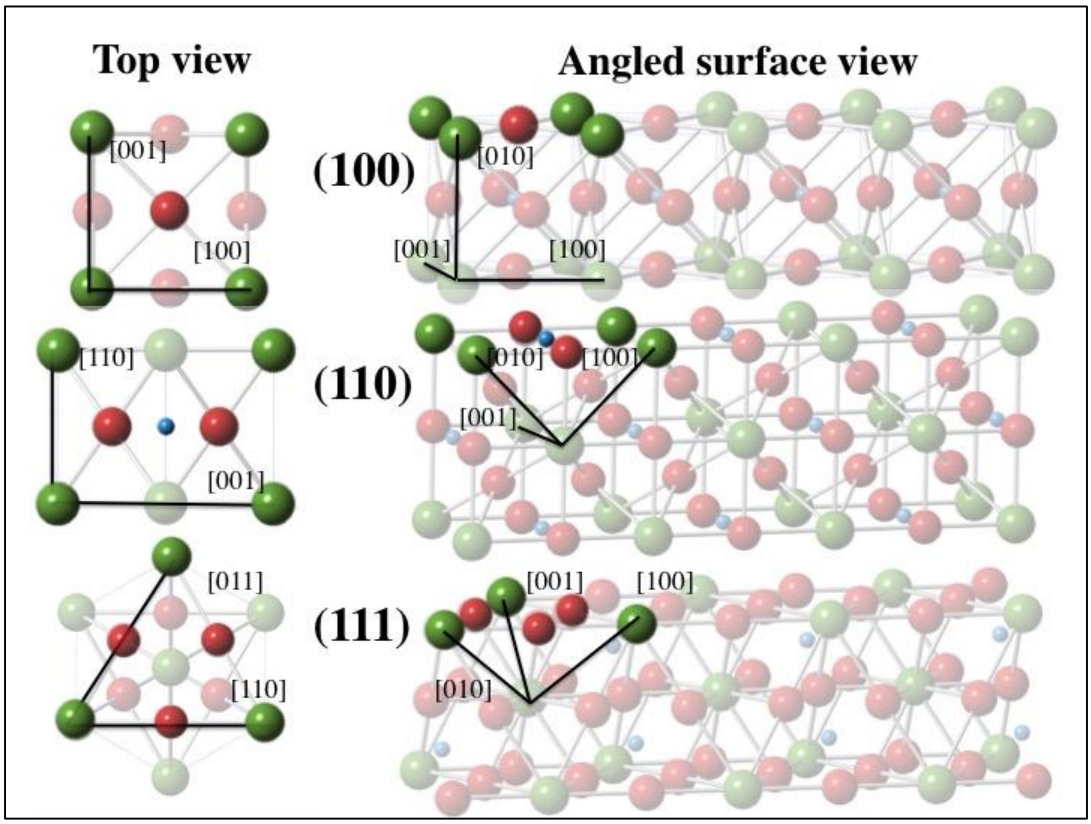

Figure 2. LAO (100), (110), and (111) directions and atomic layers are pictured. This figure shows the significance of orientation of a crystal. As described in Section 1.5, the termination layers of a crystal (i.e. the surface) are generally not as simple as the unmodified bulk atomic stacking shown here.

1.5 Surface phenomena

In the applications described above and in general, surfaces play a particularly important role in a material's effectiveness. The entire field of surface science is significant because of the unusual but functionally significant behavior of surfaces. Surfaces behave differently than the bulk of a material because of the presence of "dangling bonds," caused by the discontinuity of

the crystal structure beyond the surface. These dangling bonds cause surfaces to have a higher energy and/or a charge. Surfaces can reorganize in three ways to form more energetically favorable states:

1. Atoms and vacancies within the first few layers of the surface can rearrange, forming "surface reconstructions" (see Figure 3). Reconstructions are described in terms of their periodicity in relationship to the bulk unit cell.
2. Surfaces can adsorb atoms from the environment.
3. Electronic charge can be redistributed throughout the layers of the material closest to the surface.

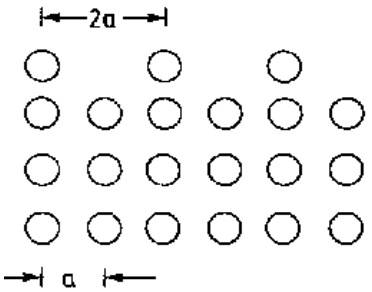

Figure 3. The simplified 2D schematic diagram represents a cross section of a crystal. The top atomic layer has a larger horizontal periodicity and a smaller vertical periodicity than the other layers. If this crystal were three-dimensional and each atomic row repeated into the page with the same structure, the periodicity of the surface would be referred to as (2x1) [24].

A few of the top-most layers of the material are involved in these surface changes, which can result in the introduction of strain fields. The development and availability of electron microscopy has made studying these few atomic layers possible. Imaging can show the presence of ordered surface structures such as faceting, steps, and terraces. In diffraction patterns of thin areas of samples, faint surface spots can be observed under certain conditions. The position and intensity of the surface spots can be used to infer surface structures. Microscopy techniques along with computational simulations allow for modeling of potential surface systems.

1.6 Past $LaAlO_3$ surface research

Most research on the composition, structure, and morphology of LAO surfaces has focused on LAO (001) and a few studies have been published about LAO (110). Atomic reconstructions are a particular area of interest for future research, so the proposed surface reconstructions for LAO (001) and (110) are reviewed below. The LAO (111) surface was studied experimentally in one publication in the context of complex oxide heterostructures, but

no published research examines surface reconstructions or other structural studies of the isolated (111) surface.

The first surface studies of $LaAlO_3$ single crystal substrates were done in an effort to improve the quality of thin film growth on LAO substrates. In 1996, Z.L. Wang reported the presence of fine structures present across large terraces on the LAO (110) surface, which contrasted with the observed atomically flat surface of the LAO (100) orientation [25]. This surface anisotropy led to further studies differentiating the structures of oriented LAO surfaces. Early surface studies also examined the relationship between micro-scale surface features and surface atomic arrangement. Wang and Shapiro studied the relationship between surface steps and reconstructed surfaces, finding that the steps were not necessary for the presence of the surface reconstruction but that they enhanced the reconstruction [26]. Steps and terraces can accompany and contribute to surface reconstructions and are therefore a notable feature in studies of LAO.

1.6.1 LAO (001)

The use of LAO (001) as a substrate for growth of thin film superconductors, such as $YBa_2Cu_3O_{7-x}$, was the earliest motivation for studies of single crystal LAO. In 1995, Wang and Shapiro studied the (001) surface in order to better understand the effect of substrate surface features on thin film growth. Using transmission electron microscopy (TEM) images of $YBa_2Cu_3O_{7-x}$, they proposed that the density of steps on LAO (001) contributed to the presence of columnar defects in the film. Using reflection electron microscopy (REM), they studied the structure of twins, surface steps, and dislocations [27]. Dislocations were found near twin boundaries but not flat areas. Norton and Bentley also studied twinning in LAO (001), but did so with un-annealed substrates. They found that twin boundaries showed a memory effect in which the boundary would move back and forth along the same path and with the same morphology when heated and cooled. They confirmed these results with both REM and *in-situ* transmission electron microscopy (TEM) [28, 29] .

A few reconstructions have been proposed for the LAO (001) surface. Wang and Shapiro observed weak diffraction spots between superlattice spots using reflection high-energy electron diffraction (RHEED) and REM, indicating the presence of a 5x5 surface reconstruction [26]. The samples they prepared were annealed at 1500°C in air for 20 hrs. Lanier et al. proposed a √5 x √5*R26.6*° (RT5) reconstruction using TEM and direct methods [30]. Recently, Krishnaswamy et

al. referred to the RT5 reconstruction as puzzling because of the high energy of the proposed delocalized holes. The researchers propose a number of other possible reconstructions, depending on the presence of hydrogen impurities, with the most stable being a 3x2 La-vacancy reconstruction on the LaO terminated surface.

The surface termination of LAO (001) is an important design consideration related to surface reconstructions. Based on Wang and Shapiro's work, the (100) face of LAO was predicted to terminate with an AlO_2 or LaO layer but not a combination of the two [27]. Kawanowa et al., using low energy neutral scattering spectroscopy, identified that the surface termination changed based on sample treatment. They found the surface termination of LAO (001) as LaO at 1000K, but mixed AlO_2 and LaO at room temperature. However if a substrate was annealed for longer periods of time prior to analysis, the surface was found to be mainly LaO terminated [31]. Researchers have also mentioned the possibility of an unreconstructed AlO_2 termination layer [32, 33]. It is clear from a number of publications that different surface terminations can be formed using different processing techniques.

1.6.2 LAO (110)

Mortada et al. produced experimental results demonstrating the presence of a c(4x2) reconstruction on LAO (110). This reconstruction was observed on samples that were annealed in UHV at 900°C for 7 hours. Additionally, terraces and facets were observed after annealing at 1500°C in air for 10-20 hours [34].

Kienzle et al. investigated LAO (110) and reported a 3x1 surface reconstruction (see Figure 4) using a combination of electron diffraction, x-ray photoelectron spectroscopy, and density functional theory [35]. This reconstruction is comparable to the STO (110) 3x1 reconstruction. The researchers are also currently investigating a 2x1 reconstruction.

1.6.3 LAO (111)

Middey et al used LAO (111) as a component of an LAO/LNO superlattice and as the substrate for the superlattice. The LAO (111) substrate, as received, was studied by AFM and XPS and found to be of mixed Al^{3+} and $(LaO_3)^{3-}$ termination and to exhibit the presence of hydroxides on the surface in order to compensate for the surface polarity [21].

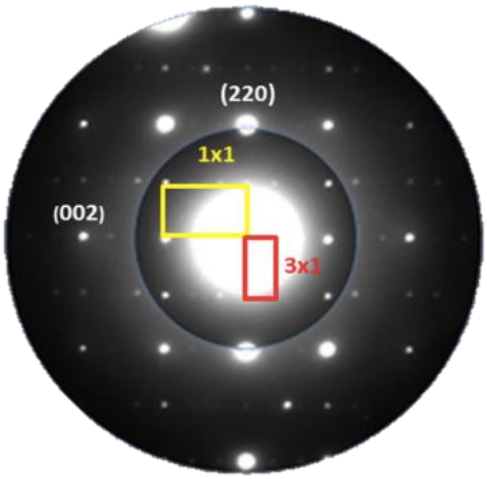

Figure 4. Transmission Electron Diffraction pattern of LAO (110) showing the 3x1 reconstructed spots (red box) compared to the typical 1x1 unit cell (yellow box) [29].

1.7 Goals of this work

As described above, the published work on LAO (111) is limited to an overview of the properties of an unmodified substrate. At the time of this writing there has been no published work exclusively focusing on the (111) surface of $LaAlO_3$ and the possible presence of reconstructions. The goal of this work is to determine whether there are interesting phenomena occurring on the surface of LAO (111). The development and now standard use of electron microscopy in materials science research presents multiple techniques that make precise surface studies of materials such as LAO possible. Combinations of microscopy, spectroscopy, and computational analysis can be used to characterize surface structures experimentally and theoretically. The following section will explain the techniques that have been used in this work to characterize the LAO (111) surface.

2. EXPERIMENTAL METHODS

This section describes the experimental methods used in the investigation of $LaAlO_3$. Significant effort was committed to the theoretical study and practical application of sample preparation and characterization techniques. Experiments were performed primarily using equipment in the Northwestern University Atomic and Nanoscale Characterization Experimental Center (NUANCE) facilities and at the University of Illinois at Chicago Electron Microscopy Service (EMS).

2.1 Single crystal sample preparation

An in-depth sample preparation process is required to make electron transparent samples for microscopy out of perovskite substrates. Figure 5 shows schematic diagrams of each stage in the preparation process. The process can be applied to a number of single crystal materials and all orientations. $LaAlO_3$ substrates of (110) and (111) orientations, 10mm by 10 mm by 0.5 mm with one side EPI polished, were purchased from MTI Corporation. The substrates were cut into 3 mm diameter discs using an Abrasive Slurry Disc Cutter and slurry of 14-µm silicon carbide powder mixed with water [36]. The discs were polished by hand using water and silicon carbide grit paper until a thickness of under 150µm was achieved. Following thinning, the sample was dimpled on both sides using a Dimpler D500i and diamond slurry until the middle (the thinnest part of the sample following dimpling) reached 20 µm [37].

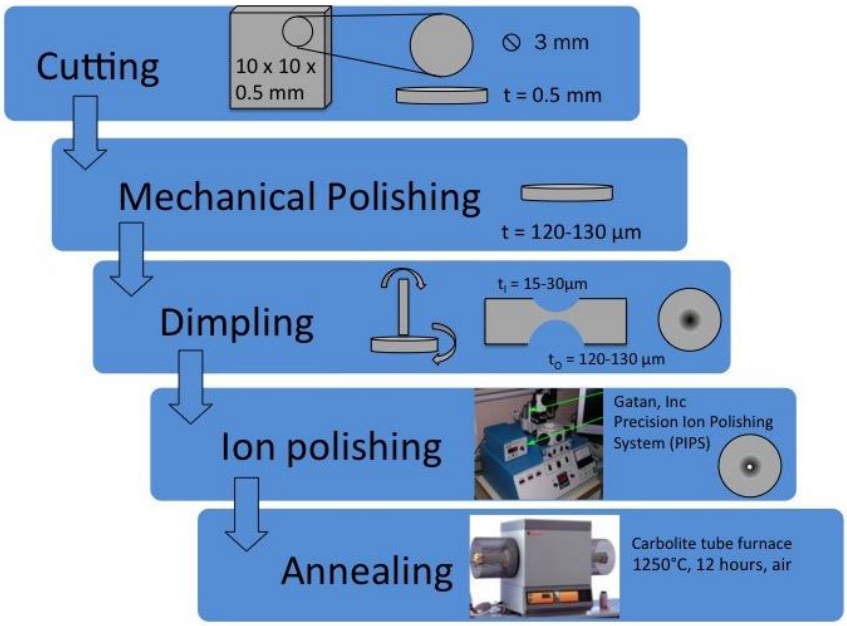

Figure 5. Schematic of single crystal sample preparation process [38].

Using various ion-polishing systems including the Precision Ion Polishing System (PIPS) from Gatan, Inc., Argon ions were directed at the sample in order to penetrate the sample, forming a central hole as well as thin areas around the hole. The ion polishing occurred at decreasing levels of intensity, with ion energy ranging from 2.0-5.5 keV, incident angle varying from 6-10°, and exposed time ranging from 2 to 8 hours. Run times and exact parameter settings would vary per sample depending on initial thickness, but a typical cycle might be as follows: 4 hours at 4.5 keV and 10° until hole observed, 30 min at 2.5 keV and 6° to further polish.

Following ion polishing, the sample was sufficiently thin but had accumulated defects, excess material, and other imperfections during the polishing procedures. Annealing is the final step that acts to clean up the surface and also to form favorable conditions for the formation of surface reconstructions and other phenomena. Two similar models of Carbolite tube furnaces were used for annealing: STF 15/51/180 (maximum temperature: 1500°C) and CTF 17/300 (maximum temperature: 1700°C) [39]. All samples were placed in alumina boats, and during most preparation procedures the boats were housed in open-ended quartz crystal tubes within the furnace tube. Section 3.2 describes observations resulting from samples that were annealed without quartz crystal tubes. Each annealing step was performed in air using ramp rates of 5-10°/min for heating and cooling and dwelling at 1230-1250°C for 12 hrs.

2.2 Transmission electron microscopy (TEM)

Optical microscopes use light, manipulated with apertures and glass lenses, to magnify samples to the micron level. Electron microscopes are principally similar, but far more complicated, powerful, and expensive. Developments in high-resolution electron microscopy have made it possible to resolve individual columns of atoms (see Figure 6). The resolution of a microscope is determined by the quality of the electron source and lenses. Electron microscopes, such as the one in Figure 7, use a beam of electrons, manipulated with apertures and electromagnetic lenses, to produce detectable scattered and transmitted electrons. There are multiple ways of processing these signals including formation of images, diffraction patterns, and various spectra. Figure 8 shows schematic optical diagrams of the TEM during formation of diffraction patterns and images.

This project used two types of electron microscopy: transmission electron microscopy (TEM) and scanning transmission electron microscopy (STEM). TEM is a method of microscopy that uses electrons transmitted through samples to produce real and reciprocal space representations of the sample. STEM utilizes principles of TEM and scanning electron microscopy (SEM) as described in more detail in section 2.3. There are a number of advantages to using TEM for perovskite surface analysis. TEM has extremely high spatial resolution and displays information by projection, which allows the user to easily and quickly view entire areas of the sample. The requirement of thin electron transparent samples for TEM and associated sample preparation process as described in 2.1 is cumbersome but unavoidable. This work involves basic plan view imaging and analysis of diffraction patterns. Experiments were

performed on the Hitachi H-8100 TEM and the JEOL 2100 FasTEM in the Electron Probe Instrumentation Center (EPIC) within NUANCE.

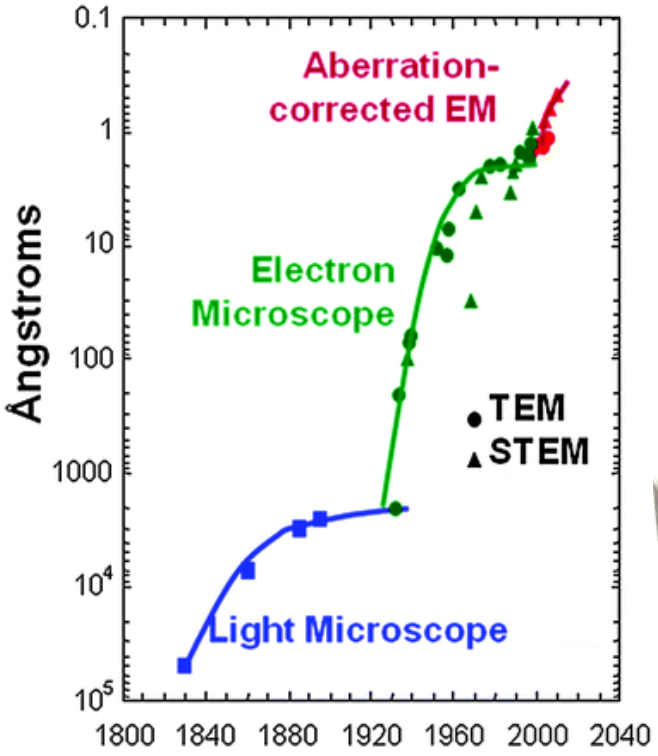

Figure 6. The spatial resolution possible with microscopy has increased over the last 200 years, with the development of the electron microscopy (TEM and STEM) and aberration correction techniques [40].

Figure 7. A TEM consists of a tall column housing the vacuum system, electron source, lenses, apertures, and specimen entry chamber. A Hitachi H-8100 TEM, which was used for much of the microscopy in this project, is shown [41].

2.2.2 Diffraction

Diffraction, one of the most complicated but useful aspects of TEM, is built upon the principles of the de Broglie relationship, Bragg's law, and the Ewald sphere construction. Extensive descriptions of diffraction theory are left to microscopy textbooks, but a summary of the formation of diffraction patterns and their significance will be sufficient for this project.

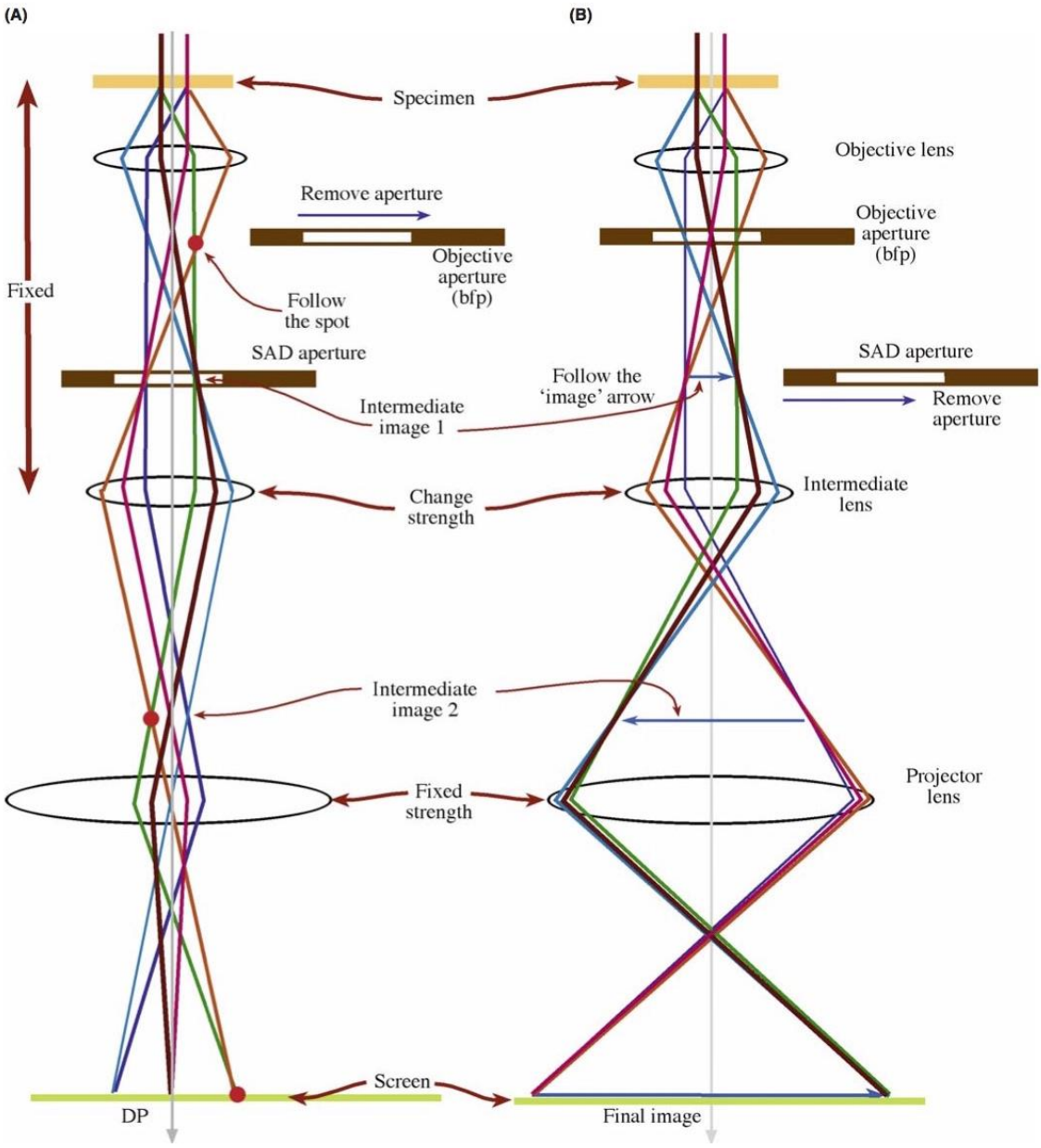

Figure 8. Diffraction mode (a) and imaging mode (b) are methods of TEM operation. Lenses and apertures are manipulated to change the path of the electron beam to form the desired output [42].

A beam of monochromatic radiation interacting with a slit will create a pattern on a parallel screen beyond the slit. Spots in this pattern are indicative of constructive interference, or in-phase interactions between light "waves." Simply, this is what is happening with electron diffraction. The incoming electron beam interacts with the sample and subsequently transmits and diffracts electrons. The electrons create a diffraction pattern on the back focal plane of the objective lens. The intensity and positioning of the spots in the diffraction pattern provide information about the sample. The distance between lattice planes of a crystalline material can be

determined by measuring the distance between the transmitted spot (the central, darkest spot of a diffraction pattern) and the diffracted spots. This process is known as indexing, and can also provide information about the phase or orientation of a crystal. Figure 9 shows example diffraction patterns of LAO (110) and LAO (111) crystals, after annealing.

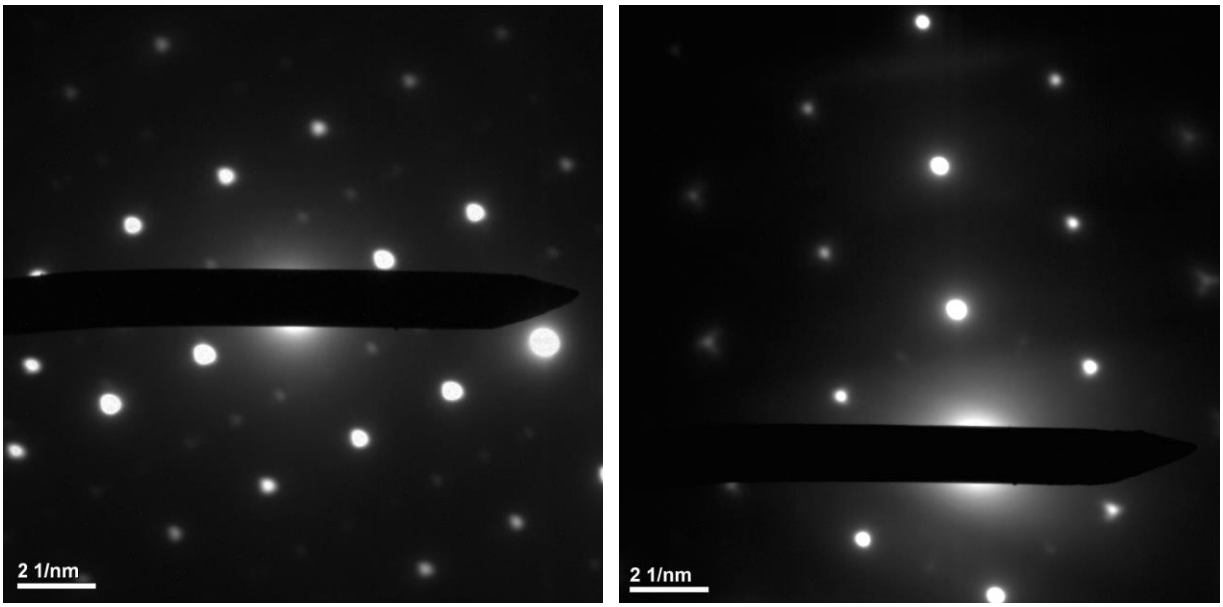

Figure 9. Diffraction patterns of a) LAO (110) and b) LAO (111) samples are shown.

2.2.3 Imaging

Changing the way the incident beam interacts with the specimen affects electron scattering, which in turn changes the type of contrast that is present in images. A brief description of simple imaging modes is sufficient for the techniques used in this project but by no means comprehensive. Adjusting the size of the objective aperture changes the amount and type of electrons that make their way to the image. Using the objective aperture to select the transmitted beam of electrons (also known as the "direct" beam) from a diffraction pattern produces a bright field (BF) image, while using it to select a diffracted beam produces a dark field (DF) image. An electron optic diagram of the difference between these two types of images is shown in Figure 10a and 10b. Centered dark field (CDF) images are formed by tilting the beam until the diffracted beam is centered, increasing the strength of signal obtained. An image taken with no beam selected by the objective aperture will be referred to as a "normal" TEM image in this work.

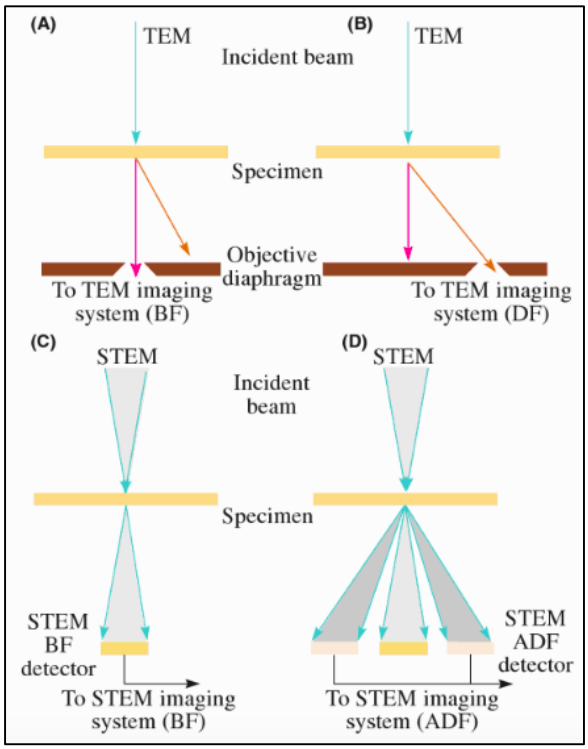

Figure 10. TEM a) bright field and b) dark field imaging involves selection of the desired beam using the objective aperture, while STEM imaging involves the use of c) BF and d) ADF detectors [42].

2.2.4 Contrast mechanisms

Image contrast mechanisms allow researchers to determine more precisely what is being shown in an image. By changing specific microscope conditions, different contrast mechanisms can be presumed dominant and conclusions about the sample can be drawn. The simplest and most omnipresent category of contrast mechanism is "amplitude contrast," formed by electron scattering due to variations in a sample's thickness. One type of amplitude contrast, mass-thickness contrast, results from incoherent elastic electron scattering, or Rutherford scattering. Mass-thickness contrast is commonly referenced in biological applications and microscopy of amorphous materials where thickness variations are particularly important for analysis. In the setting of this project, mass-thickness contrast from conventional TEM is not specific enough to provide useful information. In STEM, Z-contrast describes a high-resolution type of mass thickness contrast attainable using a High Angle Annular Dark Field (HAADF) detector. This is described in greater depth with other STEM contrast mechanisms in Section 2.3.

Diffraction contrast, a second type of amplitude contrast, is useful in the analysis of crystalline materials. Diffraction contrast is produced from coherent elastic electron scattering, or scattering that occurs at Bragg angles. Strengthening the intensity of diffraction contrast is

possible by forming a two-beam condition in which the transmitted beam and one diffracted beam in a diffraction pattern are both strong spots. Changes across the sample in crystal structure and orientation cause diffraction conditions to change, which is shown in an image by diffraction contrast.

Phase contrast is the other major type of contrast mechanism. Selecting more than one beam (instead of just one beam, as described above) forms images with phase contrast. Generally, "fringes" on TEM images are indicative of phase contrast. Lattice fringes are indicative of the local crystal structure and orientation of a specimen. Moiré fringes show a magnified view of misfit present between structures. Fresnel fringes are often visible in out-of-focus areas and can be used to study defects [42]. Phase contrast is most relevant when studying high-resolution TEM images.

2.3 Scanning transmission electron microscopy (STEM)

2.3.1 Basic principles

STEM is a microscopy technique that utilizes principles of both scanning electron microscopy (SEM) and TEM while maintaining extremely high spatial resolution. STEM utilizes information gathered from an electron beam transmitted through a sample. Additionally, STEM is capable of detecting signal from x-rays and secondary and scattered electrons.

2.3.2 Imaging capabilities and contrast mechanisms

Compared to TEM, STEM imaging is principally different, has additional capabilities, and requires different considerations regarding contrast mechanisms. As opposed to TEM image formation, which is done with a static beam and image projection, STEM imaging involves a scanning beam and electron detectors. The difference between the two is shown schematically in Figure 8. Instead of selecting transmitted or diffracted beams with apertures as in TEM, STEM detectors pick up the relevant signal from the beam at individual points as the beam scans the sample. To obtain bright field images, a bright field detector is inserted. To obtain dark field images, an annular dark field (ADF) detector is inserted around the BF detector to pick up scattered electrons. Variations in size or position of the ADF detector and, subsequently, the angle at which scattered electrons are obtained, allow users to obtain high-angle ADF (HAADF) and low-angle ADF (LAADF, or ADF) images. HAADF images are generally dominated by Z-

contrast, which is formed by electrons scattered far enough to maximize Rutherford electron scattering and reduce the effects of diffraction contrast.

2.3.2 Energy dispersive x-ray spectroscopy (EDS)

EDS (also referred to as EDX) is a technique used for measuring the relative presence of different elements in a section of a sample. An electron beam interacts with the sample, causing the emission of x-rays which are received by an EDS detector, converted into electrical voltages, and sorted into categories based on the characteristic x-ray energy of elements. EDS detectors can be integrated into SEM or STEM systems.

2.3.3 Electron energy loss spectroscopy (EELS)

EELS is another type of spectroscopy used within microscopy systems. It is complementary to EDS, but distinct. Instead of detecting characteristic x-rays as EDS does, EELS measures the energy loss that occurs after electrons interact with the specimen. EELS is especially useful for studying light elements in the periodic table because of its sensitivity.

2.4 X-ray photoelectron spectroscopy (XPS)

XPS is a method used to characterize surface composition of materials. A beam of x-rays is aimed at a certain part of a sample. The beam's interaction with the sample is limited to a shallow portion of the material, from which electrons are emitted as a result of the photoelectric effect. The kinetic energy and number of the emitted electrons are measured and displayed in spectra. Characteristic spectra for elements are known, so analysis of the spectra yields information about the elemental composition of the top portion of the sample. Adjusting the angle of the sample is possible; at increased angles, XPS measures signal that is more surface-sensitive as shown in Figure 11. The XPS used in this work was the Thermo Scientific ESCALAB 250Xi model.

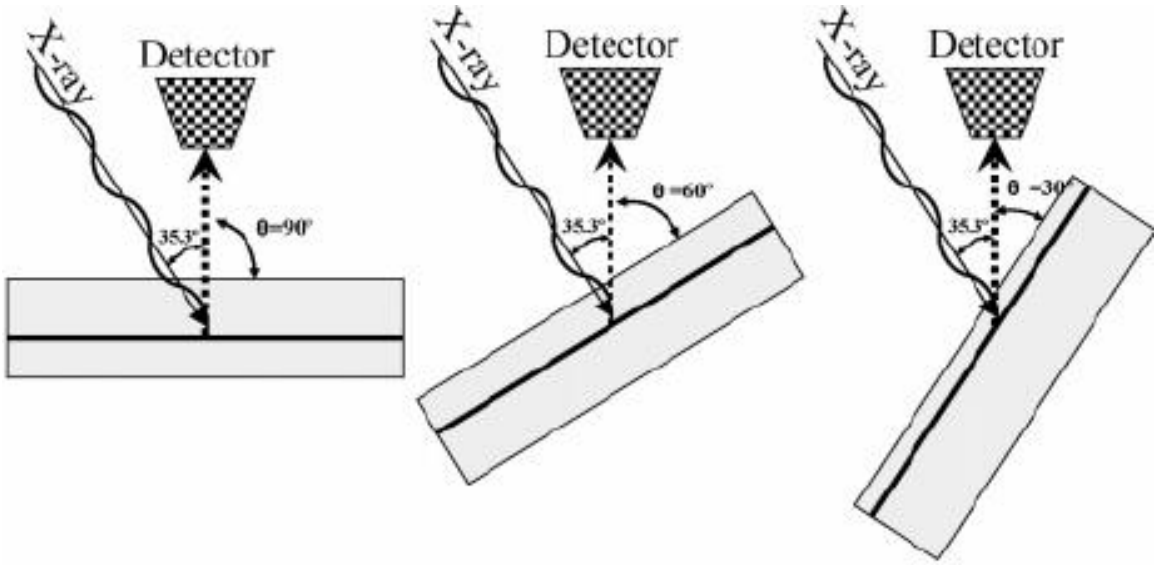

Figure 11. Angle resolved x-ray photoelectron spectroscopy changes the depth that the incoming x-rays are able to penetrate [43].

2.5 Atomic force microscopy (AFM)

Atomic force microscopy is a type of scanning probe microscopy in which a small probe oscillates over the surface of a sample. The piezoelectric interaction between the probe tip and the sample surface allows for topographical mapping of the material surface. The AFM in this work was done on a Bruker Dimension FastScan AFM.

3. RESULTS

3.1 $LaAlO_3$ (111) surface and edge features

The following section will describe the imaging work done on LAO (111) and the subsequent comparison of the LAO (111) profile edge to the LAO (110) 3x1 [35] and 2x1 (currently unpublished) reconstructions.

3.1.1 Conventional TEM

TEM images in normal, bright field, and dark field were taken of various LAO (111) samples. All samples were prepared in the methods described in Section 2.1, and were annealed for 12 hours at 1250°C in air. A selection of the images is included in addition to commentary on what they imply about the surface. Figures 12 and 13a show low magnification normal, bright field, and dark field images of LAO (111). The edges are noticeably faceted in consistent directions. Fringes are visible in the bright and dark field images, but due to the relatively low magnification, the implications of the fringes are unclear. In Figure 13a, it is also noticeable that there is a much smaller saw-tooth pattern on the edge of the sample. This smaller pattern is shown in higher magnification in Figure 13b.

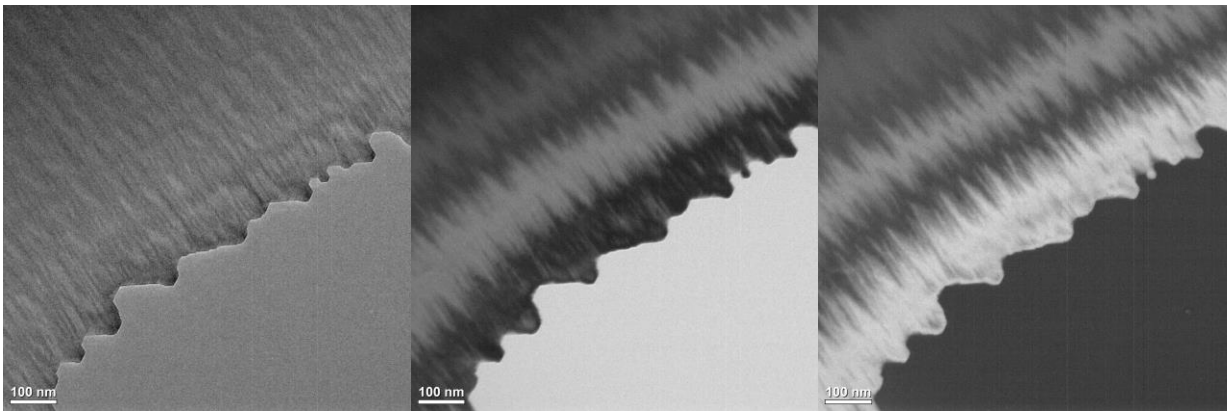

Figure 12. Low magnification a) Normal, b) Bright field, and c) Dark field TEM images. Hitachi H-8100.

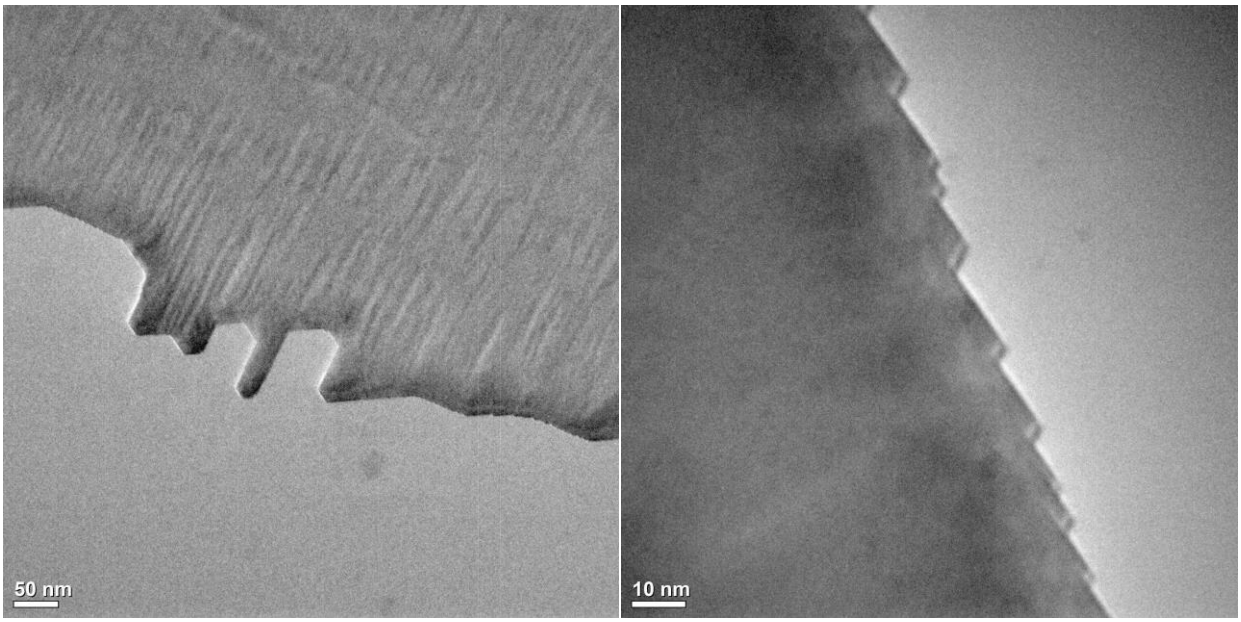

Figure 13. a) Low magnification and b) high magnification TEM images demonstrating faceted edges. Hitachi H-8100.

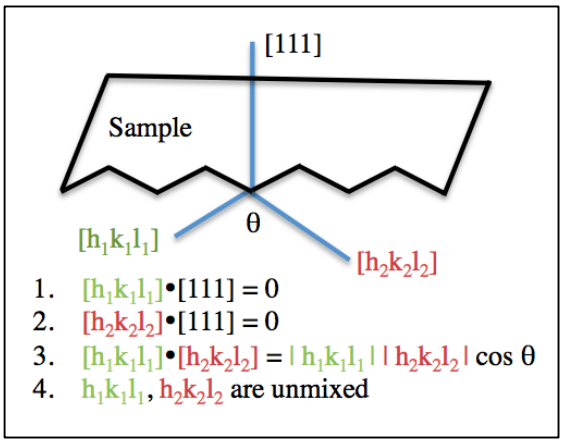

Figure 14. Geometric and mathematical relationship between facet faces and crystal orientation.

In order to identify the orientation of the preferential faceting, angles were measured in ImageJ. The most commonly observed angles in all images were 112° and 120°. Since the samples were of known (111) orientation, the directions of the facets would both be perpendicular to the [111] direction, as shown in Figure 14. The angle between two facets also describes the angle between the two facet faces, based on geometry. Also, the two unknown directions must follow the structure factor rule that the indices must be all even or all odd. A MATLAB script was written and used to calculate all possible directions given the angles listed.

The script output listed possible sets of families of planes of the edge: (220), (224) and (246) for 120° facets, and (246)/(248) for 115° facets.

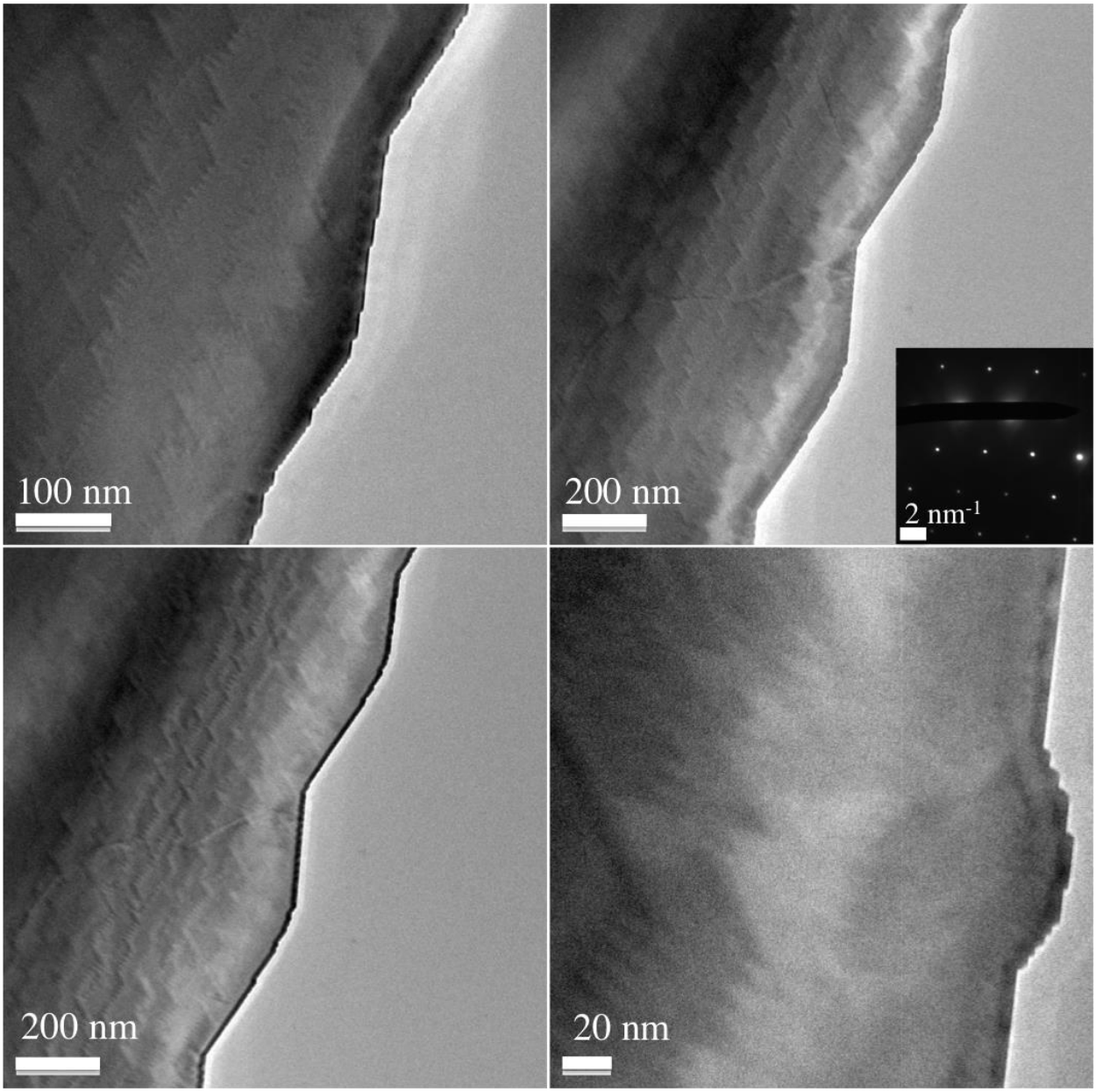

Figure 15. Normal images of LAO (111) surface: a) under-focused, b) properly focused, c) over-focused, d) high magnification, e) diffraction pattern. Hitachi H-8100.

Additionally, jagged features are observed on the LAO (111) (see Figure 15) that could imply presence of a reconstruction. Two hypotheses have been formed about the jagged features:

1) The LAO (111) surface forms steps with micro-faceted edges.
2) The jagged edges are Moiré fringes which indicate a preferential segregation of material around the step.

3.1.2 HRTEM

Conventional TEM on the H8100 microscope is not sufficient to resolve individual atomic columns, so HRTEM was performed using the JEOL 2100 FasTEM. Ahmet Gulec, a postdoctoral researcher in the Marks group, provided assistance on the instrument. The images resulting from the HRTEM experiments are shown in Figure 16a and 16b. It is clear from the images that something structurally distinct is occurring along the edge of the sample. An even more powerful microscope was needed to yield more information characterizing the edge of the sample.

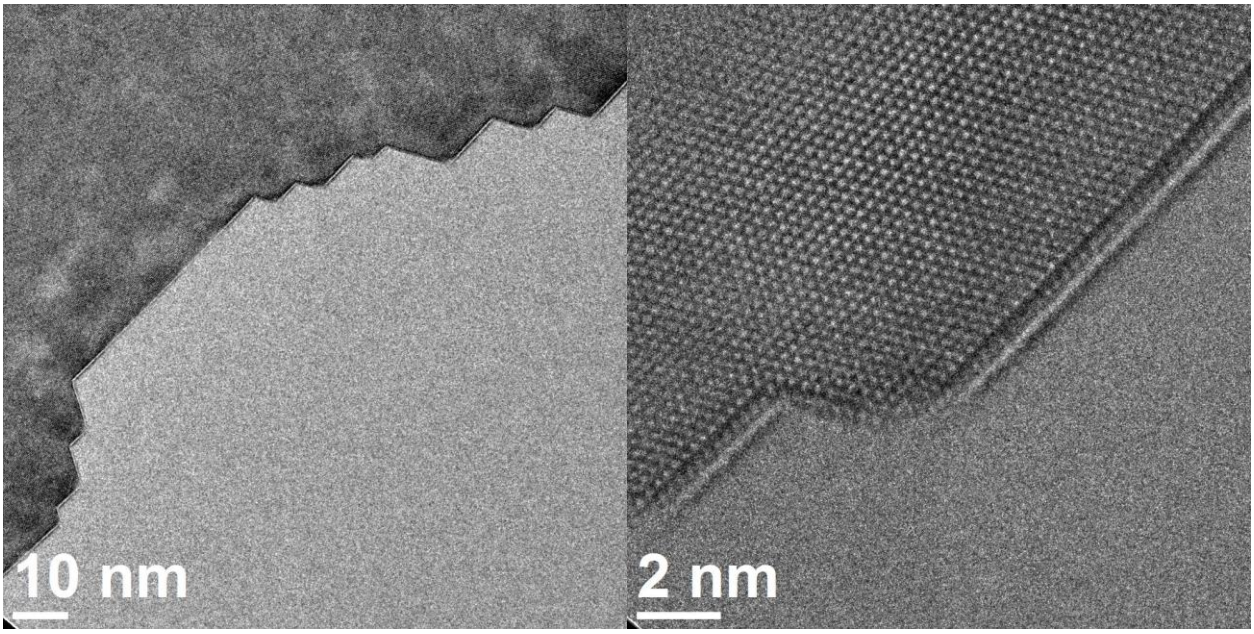

Figure 16. HRTEM images of LAO (111) surface demonstrating a) presence of faceted edges and b) a visible but not atomically resolved layer of atoms on the edge. JEOL 2100F, assisted by Dr. Ahmet Gulec.

3.1.3 STEM

Dr. Ahmet Gulec observed the LAO (111) samples with STEM, yielding sets of hundreds of images that show the distinct edge of the sample clearly. Figure 17 shows one set of images. The ABF image shows a light and dark layer beyond the last discernable set of atoms. In the bulk area of the ABF image, dark spots are lanthanum atoms. The HAADF image, dominated by Z-contrast, shows lanthanum atoms in white. The images were modified and combined in ImageJ and MATLAB to form a colored composite image (Figure 18). Prior to combination of images, lanthanum atoms appeared red in the ABF image and blue in the HAADF image. Therefore in the composite image, lanthanum columns are displayed in purple. The dark layer beyond the red and purple is the area of interest. Higher magnification images of this layer are shown in Figure

19. Since the edge layer does not look like lanthanum atoms, and given the aluminum termination of LAO (110) [35], it is probable that this edge is composed of a combination of aluminum and oxygen atoms (AlO_x). Dr. Gulec attempted EELS and EDS in an effort to elementally characterize the edge, but encountered difficulty related to the accumulation of charge of the sample and its tendency to move slightly during scans.

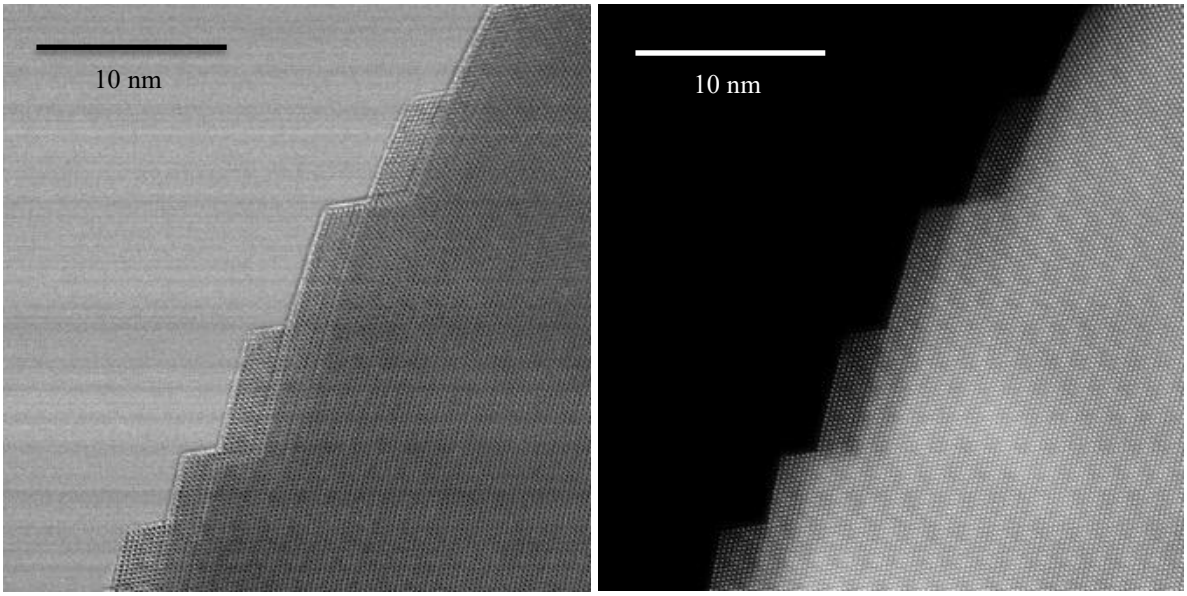

Figure 17. STEM high-resolution a) ABF and b) HAADF images of LAO (111) surface. JEM-ARM200CF, Dr. Ahmet Gulec.

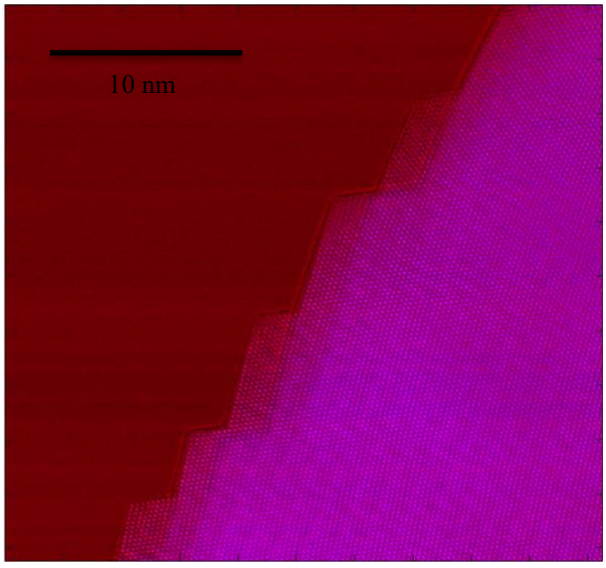

Figure 18. Composite image formed from ABF (red) and HAADF (blue) images.

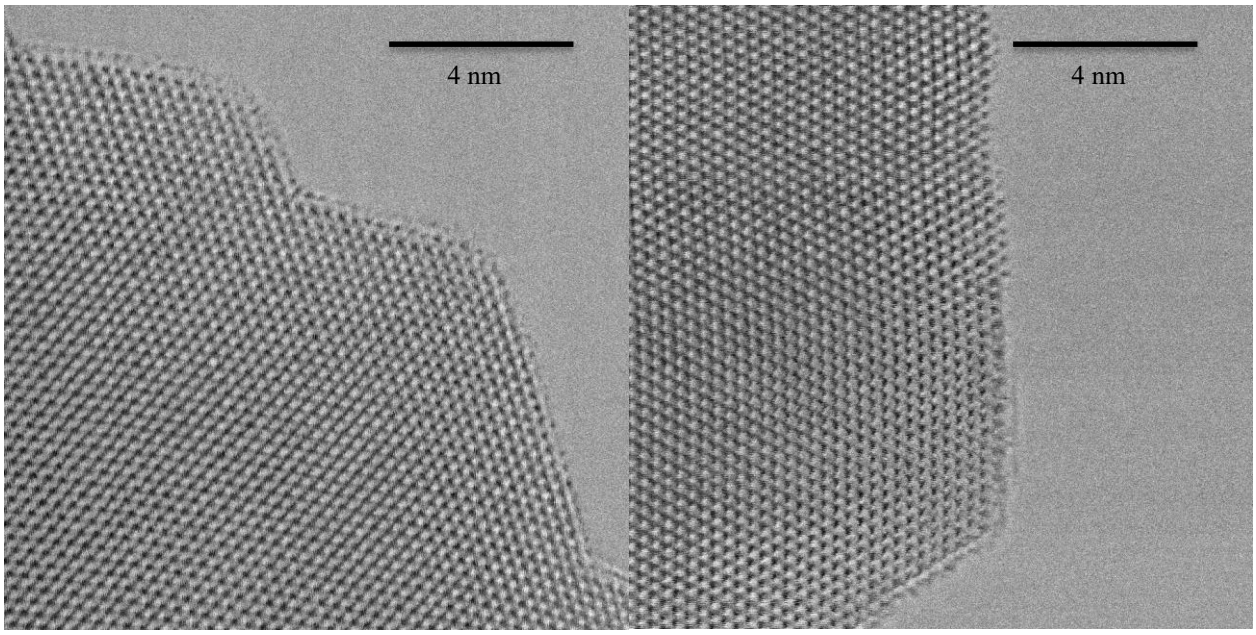

Figure 19. LAO (111) ABF images. JEM-ARM200CF, Dr. Ahmet Gulec.

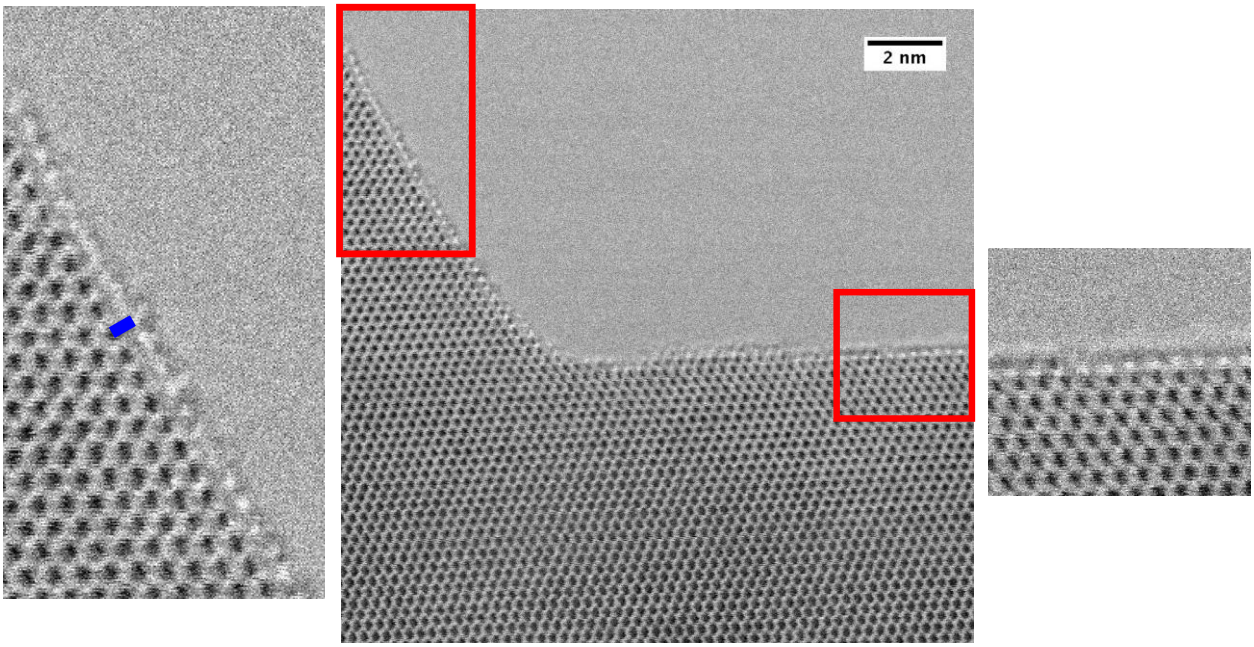

Figure 20. An ABF image of LAO (111) is shown, along with two segments of that image, 2x magnified. The blue line indicates an example of one of many measurements taken of the distance between the lanthanum atoms in black and the edge.

3.1.5 Comparison of edge to LAO (110) reconstructed surface

The ABF images from the STEM analysis show an edge with some amount of periodicity. An image of the edge is shown above in Figure 20. The distance between the black lanthanum atoms closest to the edge and the estimated middle of edge ranges between 2-3 Å. It is not possible in these images to precisely identify the location of atoms on the edge. However, the distance measurements of the edge can be compared to distance measurements in simulated reconstructed edges, proposing possible matches.

Simulations of the 3x1 and 2x1 reconstructions of the LAO (110) surface are shown in profile view in Figure 21 in order to match the configuration of this experimental work's LAO (111) sample surfaces. The 3x1 Wet C reconstruction is the most fitting of 10 simulated structures that were explored in the literature [35]. The sample preparation procedure described in the 3x1 experimental work includes an annealing step occurring at 1100-1200 °C in air for 5 hours. Four proposed 2x1 reconstructions of the LAO (110) surface are also shown in Figure 21. The experimental work accompanying these simulations involved samples that were annealed for 1050°C in air for 10 hours. Table 1 includes two different distance range estimates based off of measurements in Crystal Maker of each simulation: (1) the distance between the closest lanthanum atoms to the surface and the aluminum atoms on the surface, and (2) the distance between the lanthanum atoms and the surface oxygen atoms. These reported values are the vertical component of the distance between the atoms and are not usually representative of a bond length. The vertical component of the distance is what makes comparison between the simulation and the TEM image projections possible.

Table 1. Approximate distances between bulk and surface atoms in simulated LAO (110) reconstructions.

Reconstruction	**La/Al distance (Å)**	**La/O distance (Å)**
3x1 Wet-C	2.5-2.8	3.1-3.7
2x1 S1	2.3-2.4	2.5-2.7
2x1 S3	1.3-2.2	1.9-2.6
2x1 S4	2.3-2.7	3.4-3.6
2x1 S5	1.8-2.0	3.0-3.2

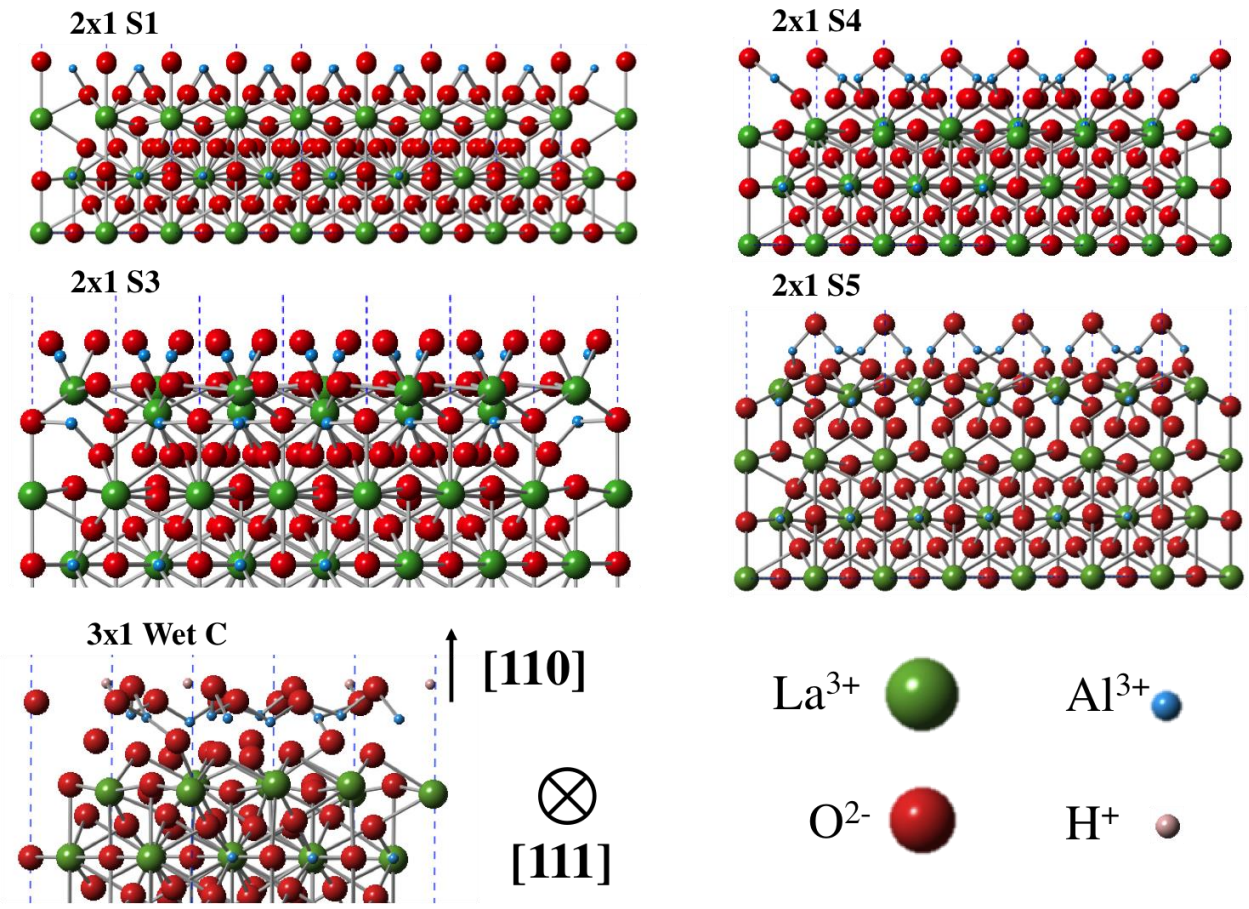

Figure 21. Simulated structures of LAO (111) with LAO (110) 2x1 and 3x1 reconstructed edges in profile view.

The annealing conditions for the samples in this work most closely match the 3x1 in temperature but the 2x1 in time, so it is not possible to distinguish which reconstruction is present. Based on comparison of the La/Al numerical measurements, the 3x1, 2x1 S1, 2x1 S4, or some combination of the structures could all reasonably be present at the (110) edge.

3.1.4 XPS

Angle-resolved XPS results demonstrated that the surface of LAO (111) is aluminum-rich. The ratio of the area under Al2p and La3d peaks is an analog for the amount of aluminum compared to the amount of lanthanum present in the area of the sample reached by x-rays. As the angle of incident x-rays in comparison to the sample surface increases, the signal detected becomes more surface sensitive. Therefore, since the aluminum-to-lanthanum ratio is increasing with angle, the LAO (111) surface must be rich in aluminum. Figure 22 shows the experimental data (dashed line) compared to a series of simulated results for different potential models of the surface. The code (modified from one used by Pratik Koirala) used known values such as mean

free paths of La and Al, predicted ionization cross-section size, and atomic spacing along the 111 plane. A layer-by-layer summation of the intensity of the La and Al peaks simulates the experimental work. Different versions of the simulation are constructed by adding different surface layers to the calculation. These three versions are displayed in Figure 22 with the experimental data which most closely matches the simulated data for a surface with an extra layer of 2.5 Al, despite the problematic jump between the 0-degree ratio and the 10-degree ratio. This is likely due to an error that does not impact the remainder of the data.

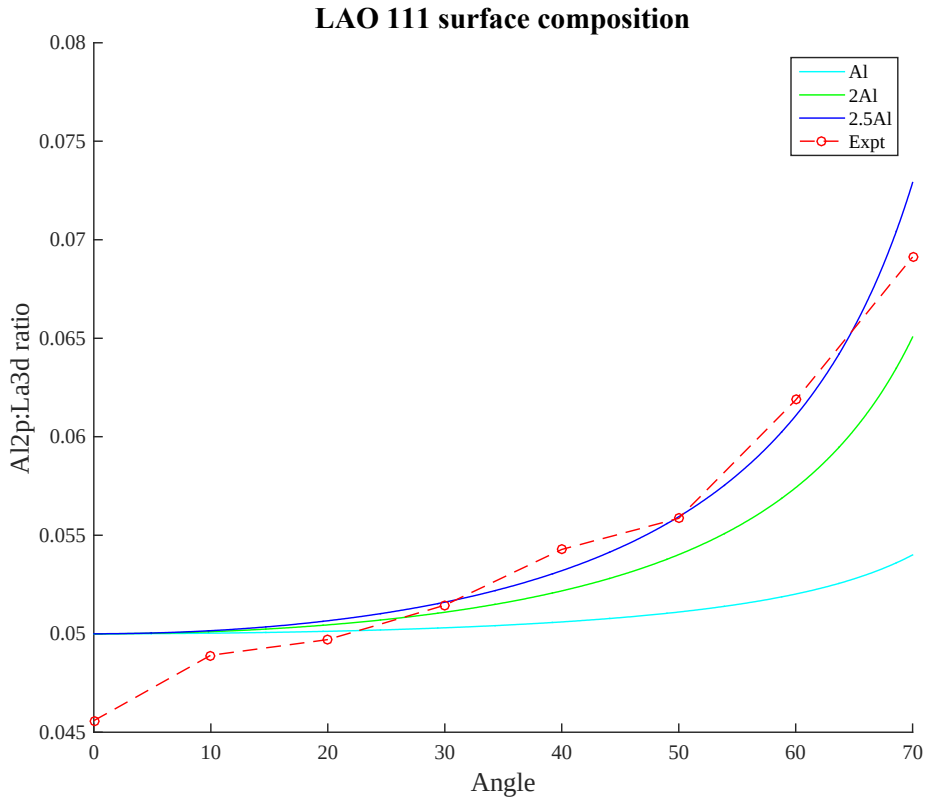

Figure 22. Comparison of experimental XPS results and simulation.

3.2 Growth of silicate particles on $LaAlO_3$ (110) and (111)

A set of LAO (110) and LAO (111) samples were prepared using a modified sample preparation procedure. The samples had already been prepared once by the usual method described in section 2.1. They were stored for multiple months, and then ion polished with low energy for 20 minutes and annealed in the tube furnace for another 12 hours at 1250°C. The samples were placed in an alumina boat for annealing, but were not housed in a quartz crystal tube. A series of unexpected results ensued. Particles of unknown origin and identity were

observed on the both LAO (110) and (111) samples. AFM confirmed that some or all particles were present on the sample surfaces. The particles ranged between circular and rod-shape. Width (defined as the smaller dimension) fairly consistently measured between 60 and 100 nm and length stretched as long as 900 nm, though usually was under 500 nm. TEM images of the particles are shown in Figure 23. The areas of the surfaces without particles appear unmodified by the presence of the particles.

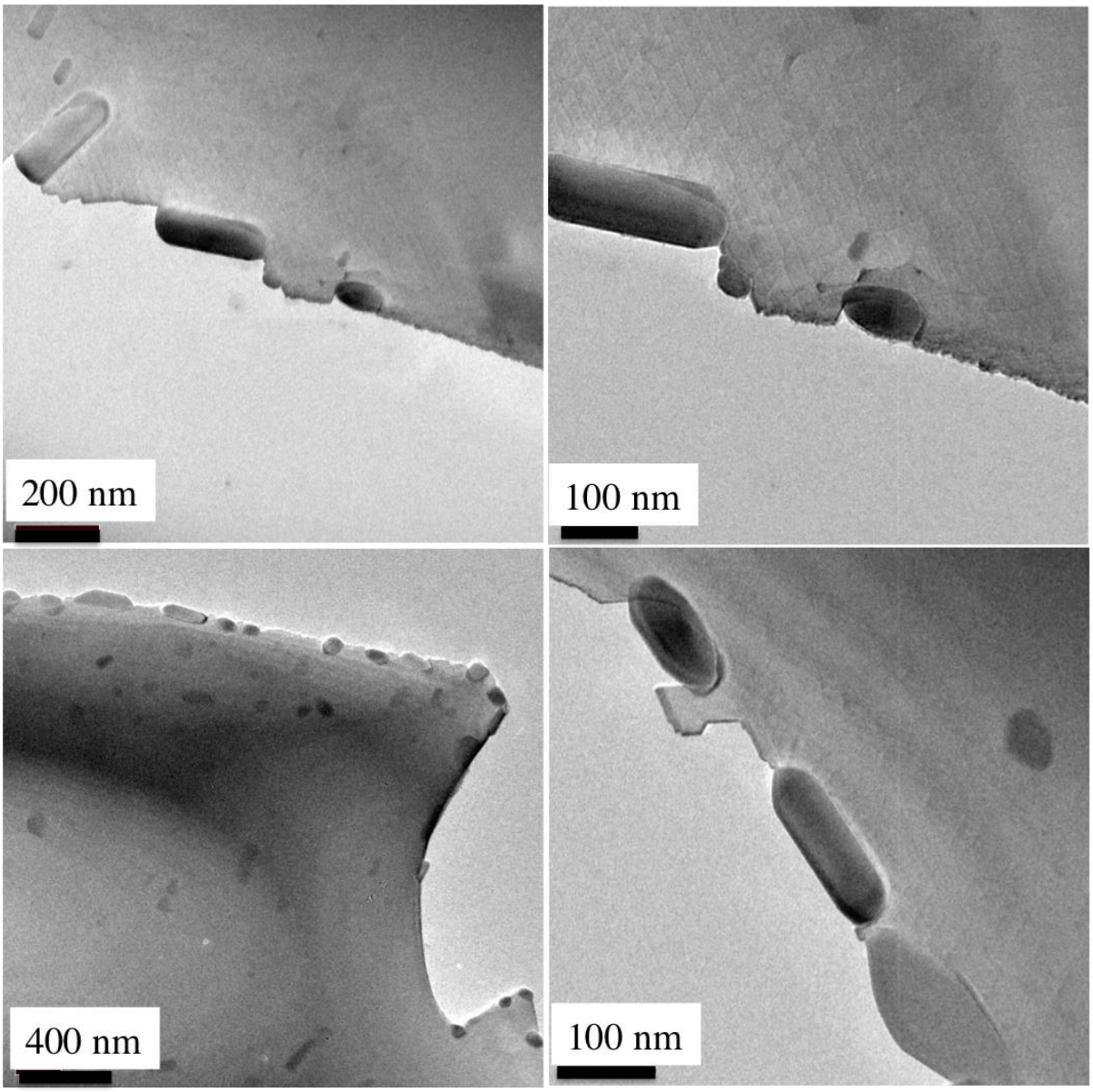

Figure 23a-d. Rod-shaped silicate particles like the ones pictured are observed on both the LAO (110) and LAO (111) surfaces after extended exposure to the inside of the furnace tube during annealing.

Dr. Ahmet Gulec studied the samples with particles using the JEM-ARM200CF. The EDS results from his work are shown below in Figure 24. The results show that the particles, rather than being purely lanthanum-rich, would be better described as "aluminum-deficient silicates." Around many particles there is a region in which silicon and oxygen preferentially diffuse into an area, displacing aluminum from that area. Some particles observed are small while others are large, leading to the prediction that during the annealing process the particles were forming and growing. Upon cooling, the particles no longer form or grow.

The observation of these particles and particularly their modes of preferential growth are interesting, but not reproducible and therefore have not been analyzed further. A word of caution is issued to future researchers to prioritize the cleanliness of the sample preparation process, especially during the annealing stages.

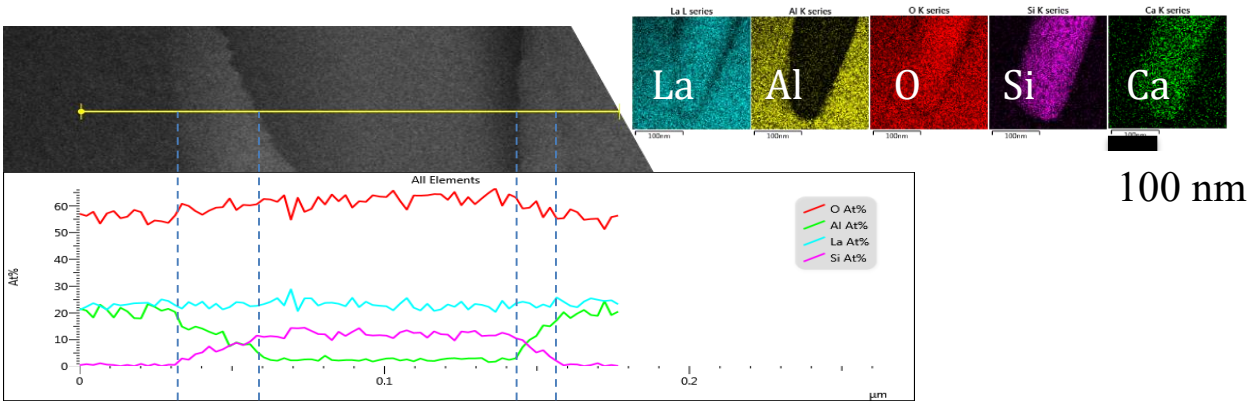

Figure 24. EDS results demonstrate the presence of silicon within the particles as well as a heightened concentration of oxygen and depleted concentration of aluminum. The calcium shown in the compositional color map is a trace amount and can be neglected.

4. CONCLUSION

Various electron microscopy and spectroscopy techniques have been used to study the LAO (111) surface. This preliminary work has demonstrated a potential reconstruction on the (111) surface and presented evidence of an nx1 reconstruction along the LAO (110) surface on the faceted (111) edge. This work has taken steps toward solving the LAO (111) surface and supplements current studies by Pratik Koirala of the 2x1 reconstructions of LAO (110).

The surface of LAO (111) is aluminum-rich and terminated with more than one AlO_x layer. The surface has features that could either be actual micro-faceted edges along steps of the surface or Moiré fringes, implying preferential segregation of atoms toward the step edges. The

faceted edge of LAO (111) shows the presence of one or more layers of aluminum that are distinctly visible from HRTEM and STEM images. The results of this work can be used in the future along with extensive diffraction studies and use of DFT to present potential surface structures of LAO (111). Knowledge of these structures can be used to optimize catalytic processes and gain a better understanding of the electronic properties of heterostructures involving LAO (111).

SUPPLEMENTARY MATERIALS

1. 2x1 s1.cif
2. 2x1 s3.cif
3. 2x1 s4.cif
4. 2x1 s5.cif
5. 3x1 Wet C.cif

Different LAO (110) reconstructed surfaces were found to form on the faceted LAO (111) edge. The model of the 3x1 reconstruction that was determined most fitting by the literature [35] is included along with four potential 2x1 reconstructions that have yet to be published. These files were provided by Pratik Koirala and used for my analysis in this project.

6. xps peak simulation.m

The MATLAB code used to form simulations of XPS data is included. Within the code, the raw XPS data are included and plotted with the simulations. Pratik Koirala provided the original code. The version included here is the one I modified for LAO (111) by changing the materials parameters and the atomic stacking within the iterative loops.

REFERENCES

1. Image modified from: https://upload.wikimedia.org/wikipedia/commons/9/9a/Perovskite.svg
2. Agency, I.E., *Technology Roadmap: Energy and GHG Reductions in the Chemical Industry via Catalytic Processes*. 2013.
3. Ulla, E.A.L.a.M.A., *Perovskite Oxides in Catalysis: Past, Present and Future.* Research on Chemical Intermediates, 1998. **24**(5): p. 581-592.
4. Yamamoto, T., T. Tanaka, T. Matsuyama, T. Funabiki, and S. Yoshida, *Structural analysis of La/Al2O3 catalysts by La K-edge XAFS.* Journal of Synchrotron Radiation, 2001. **8**: p. 634-636.
5. Liu, S.L., G.X. Xiong, W.S. Yang, L.Y. Xu, G. Xiong, and C. Li, *Partial oxidation of ethane to syngas over nickel-based catalysts modified by alkali metal oxide and rare earth metal oxide.* Catalysis Letters, 1999. **63**(3-4): p. 167-171.
6. Valden, M., R.L. Keiski, N. Xiang, J. Pere, J. Aaltonen, M. Pessa, T. Maunula, A. Savimaki, A. Lahti, and M. Harkonen, *Reactivity of Pd/Al2O3, Pd/La2O3-Al2O3 and Pd/LaAlO3 catalysts for the reduction of NO by CO: CO and NO adsorption.* Journal of Catalysis, 1996. **161**(2): p. 614-625.
7. Imai, H. and T. Tagawa, *OXIDATIVE COUPLING OF METHANE OVER LAALO3.* Journal of the Chemical Society-Chemical Communications, 1986(1): p. 52-53.
8. Ozawa, M., S. Suzuki, and H. Toda, *High-temperature automotive catalytic nitrogen oxide reduction over copper-lanthanum-alumina.* Journal of the American Ceramic Society, 1997. **80**(8): p. 1957-1964.
9. Zhu, J., H. Li, L. Zhong, P. Xiao, X. Xu, X. Yang, Z. Zhao, and J. Li, *Perovskite Oxides: Preparation, Characterizations, and Applications in Heterogeneous Catalysis.* Acs Catalysis, 2014. **4**(9): p. 2917-2940.
10. Chen, B.-R., C. George, Y. Lin, L. Hu, L. Crosby, X. Hu, P.C. Stair, L.D. Marks, K.R. Poeppelmeier, R.P. Van Duyne, and M.J. Bedzyk, *Morphology and oxidation state of ALD-grown Pd nanoparticles on TiO2- and SrO-terminated SrTiO3 nanocuboids.* Surface Science, 2016. **648**: p. 291-298.
11. Hodes, G., *Perovskite-Based Solar Cells.* Science, 2013. **342**(6156): p. 317-318.
12. Eom, D., C.S. Hwang, H.J. Kim, M.H. Cho, and K.B. Chung, *Thermal annealing effects on the atomic layer deposited LaAlO(3) thin films on Si substrate.* Electrochemical and Solid State Letters, 2008. **11**(7): p. G33-G36.
13. Jun, J.H., H.J. Kim, and D.J. Choi, *Effect of hydration on the properties of lanthanum oxide and lanthanum aluminate thin films.* Ceramics International, 2008. **34**(4): p. 957-960.
14. Suzuki, M., *Comprehensive Study of Lanthanum Aluminate High-Dielectric-Constant Gate Oxides for Advanced CMOS Devices.* Materials, 2012. **5**(3): p. 443-477.
15. Ohtomo, A. and H.Y. Hwang, *A high-mobility electron gas at the LaAlO3/SrTiO3 heterointerface.* Nature, 2004. **427**(6973): p. 423-426.
16. Gariglio, S., N. Reyren, A.D. Caviglia, and J.M. Triscone, *Superconductivity at the LaAlO3/SrTiO3 interface.* Journal of Physics-Condensed Matter, 2009. **21**(16).
17. Herranz, G., F. Sanchez, N. Dix, M. Scigaj, and J. Fontcuberta, *High mobility conduction at (110) and (111) LaAlO3/SrTiO3 interfaces.* Scientific Reports, 2012. **2**.
18. Brinkman, A., M. Huijben, M. Van Zalk, J. Huijben, U. Zeitler, J.C. Maan, W.G. Van der Wiel, G. Rijnders, D.H.A. Blank, and H. Hilgenkamp, *Magnetic effects at the interface between non-magnetic oxides.* Nature Materials, 2007. **6**(7): p. 493-496.
19. Doennig, D., W.E. Pickett, and R. Pentcheva, *Confinement-driven transitions between topological and Mott phases in (LaNiO3)(N)/(LaAlO3)(M)(111) superlattices.* Physical Review B, 2014. **89**(12).
20. Rueegg, A., C. Mitra, A.A. Demkov, and G.A. Fiete, *Electronic structure of (LaNiO3)(2)/(LaAlO3)(N) heterostructures grown along 111.* Physical Review B, 2012. **85**(24).
21. Middey, S., D. Meyers, M. Kareev, E.J. Moon, B.A. Gray, X. Liu, J.W. Freeland, and J. Chakhalian, *Epitaxial growth of (111)-oriented LaAlO3/LaNiO3 ultra-thin superlattices.* Applied Physics Letters, 2012. **101**(26).

22. da Silva, C.A. and P.E.V. de Miranda, *Synthesis of LaAlO3 based materials for potential use as methane-fueled solid oxide fuel cell anodes.* International Journal of Hydrogen Energy, 2015. **40**(32): p. 10002-10015.
23. Wang, W., L. Zhang, S. Fang, H. Xu, Y. Zhong, and Z. Mao, *Low-Emitting Property of Lanthanum Aluminate and Its Application in Infrared Stealth.* Science of Advanced Materials, 2015. **7**(8): p. 1649-1656.
24. Schematic diagram from: http://www.uni-ulm.de/fkp/lehre/gl5/ComKurs1/pict2/RECON-BC.gif
25. Wang, Z.L., *Steps and facets on annealed LAlO(3){100} and {110} surfaces.* Surface Science, 1996. **360**(1-3): p. 180-186.
26. Wang, Z.L. and A.J. Shapiro, *STUDIES OF LAALO3(100) SURFACES USING RHEED AND REM .2. 5X5 SURFACE RECONSTRUCTION.* Surface Science, 1995. **328**(1-2): p. 159-169.
27. Wang, Z.L. and A.J. Shapiro, *STUDIES OF LAALO3(100) SURFACES USING RHEED AND REM .1. TWINS, STEPS AND DISLOCATIONS.* Surface Science, 1995. **328**(1-2): p. 141-158.
28. Norton, M.G. and R.R. Biggers, *IN-SITU TRANSMISSION ELECTRON-MICROSCOPY OBSERVATIONS OF TWINNING IN LANTHANUM ALUMINATE.* Scripta Metallurgica Et Materialia, 1995. **32**(4): p. 481-485.
29. Norton, M.G. and J. Bentley, *Reflection electron microscopy observations of twinning in LaAlO3.* Journal of Materials Science Letters, 1996. **15**(21): p. 1851-1853.
30. Lanier, C.H., J.M. Rondinelli, B. Deng, R. Kilaas, K.R. Poeppelmeier, and L.D. Marks, *Surface Reconstruction with a Fractional Hole: (sqrt[5] x sqrt[5])R26.6 degrees LaAlO3 (001).* Phys Rev Lett, 2007. **98**(8): p. 086102.
31. Kawanowa, H., H. Ozawa, M. Ohtsuki, Y. Gotoh, and R. Souda, *Structure analysis of LaAlO3(001) surfaces by low energy neutral scattering spectroscopy.* Surface Science, 2002. **506**(1-2): p. 87-92.
32. Krishnaswamy, K., C.E. Dreyer, A. Janotti, and C.G. Van de Walle, *Structure and energetics of LaAlO3 (001) surfaces.* Physical Review B, 2014. **90**(23).
33. van der Torren, A.J.H., S.J. van der Molen, and J. Aarts, *Formation of a mixed ordered termination on the surface of LaAlO3(001).* Physical Review B, 2015. **91**(24).
34. Mortada, H., M. Derivaz, D. Dentel, and J.-L. Bischoff, *Structural investigation of the LaAlO(3)(110) surface.* Thin Solid Films, 2008. **517**(1): p. 441-443.
35. Kienzle, D., P. Koirala, and L.D. Marks, *Lanthanum aluminate (110) 3 x 1 surface reconstruction.* Surface Science, 2015. **633**: p. 60-67.
36. Abrasive Slurry Disc Cutter (Model 360) and 14 um powder from South Bay Technologies, Inc. http://www.southbaytech.com/shop/360.shtml
37. Dimpler (Model D500i) from South Bay Technologies, Inc. http://www.southbaytech.com/shop/D500i.shtml. Diamond slurry (1-M-WSS 159) from Wendt Dunnington.
38. Embedded images from: http://www.emc.missouri.edu/pdf/manuals/Model691.pdf and http://www.keison.co.uk/products/carbolite/tzf3.jpg
39. Tube furnaces: http://www.carbolite-gero.com/products/tube-furnace-range/universal-tube-furnaces/ctf-17-tzf-17/ and http://www.carbolite-gero.com/products/tube-furnace-range/universal-tube-furnaces/stf-15-tzf-15/
40. Yang, J.C.S., Matthew W; Grieshaber, Ross V; and Nuzzo, Ralph G., *Recent developments and applications of electron microscopy to heterogeneous catalysis.* Chemical Society Reviews, 2012. **41**: p. 8179-8194.
41. Image from: http://www.nuance.northwestern.edu/epic/instruments-epic/tem/index.html
42. David B. Williams, C.B.C., *Transmission Electron Microscopy: A Textbook for Materials Science*. 2nd ed. 2009, New York: Springer.
43. Schneider, T.A., Kateryna; Fulghum, Julia E.; Broadwater, Laurie; Smith, Ashley; and Lavrentovich, Oleg D., *Oriented Monolayers Prepared from Lyogropic Chromonic Liquid Crystal.* Langmuir, 2005. **21**: p. 2300-2307.